Draft version October 1, 2026
Typeset using LaTeX **twocolumn** style in AASTeX7.0.1

arXiv:2609.38590v1 [astro-ph.HE] 29 Sep 2026

Chandra X-ray spectral evidence of the dual AGN nature of the gravitational lens MG B2016+112 at $z = 3.273$ with 175 pc separation.

Daniel A. Schwartz [1], Júlia M. Sisk-Reynés [1,2] and Anna Barnacka [1]

[1] *Center for Astrophysics | Harvard & Smithsonian, 60 Garden St, Cambridge, MA 02138, USA*
[2] *Department of Physics, University of Maryland Baltimore County, 1000 Hilltop Cir, Baltimore, MD 21250, USA*

(Received; Revised; Accepted October 1, 2026)

ABSTRACT

We use a new 175 ks *Chandra* X-ray observation of the $z = 3.273$ radio-loud gravitational lens system MG B2016+112 to present definitive X-ray spectral evidence that it contains a dual active galactic nucleus (AGN). With a projected separation of 175 parsecs, this is the tightest separation confirmed AGN pair at high redshift. Prior multi-epoch very long baseline interferometry (VLBI) and archival *Chandra* data had revealed two distinct emitters, but could not rule out a single AGN with a complex, highly magnified jet. Our new *Chandra* observations allow a separate spectral analysis of each source. We find strong intrinsic absorption ($N_{\rm H} > 4 \times 10^{22}{\rm cm}^{-2}$, 3σ confidence) at the source redshift for the highly magnified source inside the caustic. This identifies it as an obscured AGN. In addition to the previously known type II AGN outside the caustic, this confirms a compact dual AGN system in MG B2016+112. On-going and future surveys using facilities such as *Euclid*, *SKA*, and the *Rubin* and *Roman* observatories will uncover more such systems, probing SMBH evolution and gravitational wave precursors.

Keywords: Strong gravitational lensing — Black hole physics: supermassive black holes — Active galactic nuclei: quasars ([HB89] 2016+112) — X-ray active galactic nuclei

1. INTRODUCTION

Hierarchical models of galaxy formation posit that major galaxy mergers drive the assembly and activation of supermassive black holes (SMBHs). Mergers can fuel active galactic nuclei (AGN) and regulate star formation, activity that peaked during cosmic noon ($z \sim 2-3$; P. F. Hopkins et al. 2008; T. Di Matteo et al. 2008). In major mergers each galaxy is expected to have a SMBH, so that the merged galaxy will contain a pair of black holes. To identify such pairs, both must be in a luminous active state. Direct evidence for dual AGN at high redshifts remains scarce, with confirmed pairs limited to separations of several kiloparsecs or more (Y.-C. Chen et al. 2022; F. Mannucci et al. 2022, 2023; Q. Li et al. 2025; M. Perna et al. 2025). This observational gap stems from angular resolution limits: even the Hubble Space Telescope (HST) struggles below $\sim$ 50 milliarcseconds (mas) (Space Telescope Science Institute 2023), corresponding to $\sim$ 400 pc at $z = 3$, rendering sub-kpc pairs difficult to discover via direct imaging.

Gravitational lensing mitigates this spatial resolution limit, acting as a telescope to boost spatial resolution and to reveal otherwise inaccessible structures (A. Barnacka 2018, 2017). For lensing configurations with a source within and near to the inner caustic of a lens, magnifications can exceed hundreds, spatially amplifying compact features such as 10 – 1000 pc scale jets and outflows, and revealing dual AGN.

The radio-loud source MG B2016+112[3] at $z = 3.273$ exemplifies this potential: primarily lensed by a foreground galaxy at $z = 1.01$ (D. P. Schneider et al. 1986), it features a fold caustic that quadruply images a source inside and near to the caustic with magnification of a factor $\mu \sim 350$, while doubly imaging another source that is outside the caustic (C. Spingola et al. 2019). We will refer to these as "source 1", and "source 2", respec-

Corresponding author: Daniel A. Schwartz
das@cfa.harvard.edu

[3] We will use the discovery name MG B2016+112 in this paper. In J2000 coordinates the system would be centered at J201918.1+112713.

tively, following the designation of D. Schwartz et al. (2021).

The presence of an AGN in the system was historically determined using both optical and radio observations D. P. Schneider et al. (1986). Subsequent optical spectroscopy one of the images of source 2 showed emission lines broadened by 500-900 km s^{-1} indicative of photo-ionization complexity, and revealing source 2 is a type II AGN (T. Yamada et al. 2001; L. V. E. Koopmans et al. 2002). T. Yamada et al. (2001) also detected Ly-alpha, CIII], HeII], CIV] and NV] in image C. However, T. Yamada et al. (2001) interpreted MG B2016+112 as being a single AGN, with image C being the narrow-line emission region of this single AGN. Later, source-plane reconstruction using multi-epoch VLBI observations favored the interpretation that this multiply-imaged system is comprised of two jetted radio sources (each with a flat- and a steep-spectrum component) separated by a projected distance of 175 pc at the source redshift (0.″022) (C. Spingola et al. 2019). C. Spingola et al. (2019) measured proper motions perpendicular to each other for the two radio sources, and different spectral indices, strengthening the dual AGN hypothesis. However, the interpretation of a single AGN outside the caustic (source 2; model-predicted magnification $\mu \sim 2$) with a jet crossing the caustic and producing highly magnified knots mimicking the second core (that of source 1; magnification $\mu \sim 350$) could not be ruled out, as suggested by L. V. E. Koopmans et al. (2002) and discussed by C. Spingola et al. (2019).

Astrometric analysis exploiting non-linear angular amplification by gravitational lensing and using an archival 7.8 ks *Chandra* observation confirmed two separate X-ray emission regions consistent with the two VLBI sources (D. Schwartz et al. 2021). However, with only 24 photons, the spectral analysis of D. Schwartz et al. (2021) lacked statistical power to measure intrinsic absorption from surrounding gas in the vicinity of the SMBH, thus distinguishing an AGN from jet knots (which are typically unabsorbed; F. Massaro et al. 2011).

Since source 2 was already known to be an AGN, the key to the investigation was achieving sufficient statistical power to detect absorption toward source 1, whose AGN nature had not previously been confirmed. Here, we present a new 175 ks *Chandra* dataset, revealing spectra that resolve this long-standing debate and anchor models of high-z SMBH mergers.

We use $H_0 = 67.4$ km s^{-1} Mpc^{-1}, $\Omega_{\rm m} = 0.315$, and $\Omega_\Lambda = 0.685$ (Planck Collaboration et al. 2020) throughout our analysis.

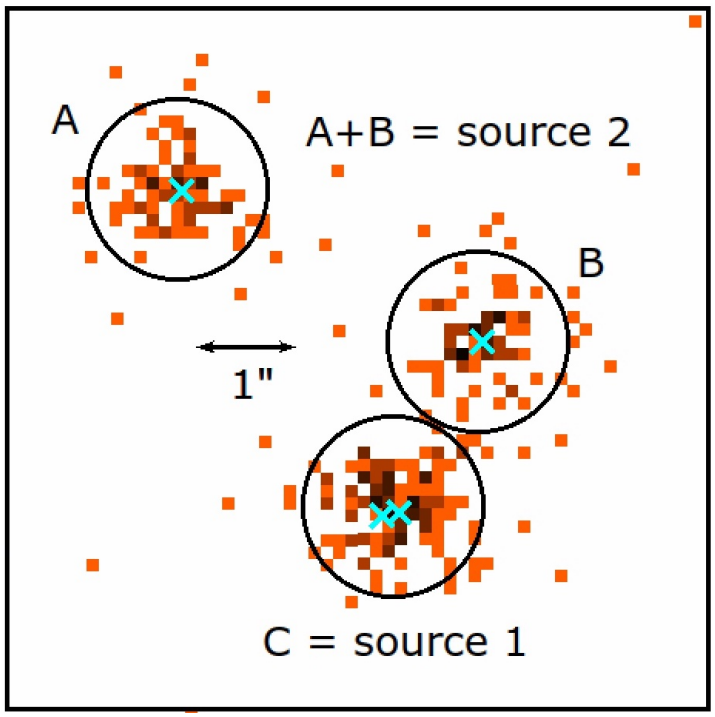


Figure 1. The image plane merged data of the 165 ks live time observation of MG B2016+112. The box shows a 7″× 7″region around the lensed images. The circles around each image have an 0.″90 radius, approximately the 80% encircled counts radius over the 0.5 – 7 keV band, as determined by an SAOTrace (D. H. Jerius et al. 2004) plus Marx (J. E. Davis et al. 2012) simulation of the individual measured image spectra (A–C) over this band. The ACIS-S3 0.5 – 7 keV data is binned into 1/4 CCD pixels, 0.″123 on a side, where orange (black) pixels show 1 (6) counts per bin. White space has zero counts. Background is approximately 0.0025 counts per 1/4 pixel bin. The cyan crosses show where the *Chandra* aspect solution gives the ICRS coordinates of the VLBI components (cf. C. Spingola et al. 2019). These offsets from the X-ray centroids are consistent with the absolute celestial location accuracy of *Chandra*.

2. *Chandra* OBSERVATIONS

To address the question of whether source 1 presents intrinsic X-ray absorption at sufficient statistical significance (which would rule out its radio jet interpretation and subsequently confirm its AGN nature), we obtained a 175 ks (165 ks live time) *Chandra* observation (∼22× longer than the archival). The data were obtained via 10 separate pointings over a fifteen-month period from December 2023 through March 2025 (doi:10.25574/cdc.436). Table 1 lists parameters of the 10 new *Chandra* observations.

At the half-arcsecond angular resolution of *Chandra* this system consists of three well resolved images, with source 2 lensed into images A and B separated by ∼3.″4, and source 1 lensed into two images that are unresolved

in image C (overlapping cyan crosses in Figure 1), about ∼2.″0 from the X-ray image B in Figure 1. The remaining two images of source 1 are very near A and B, but too faint to resolve.

The first 7.8 ks *Chandra* observation of MG B2016+112 was used to estimate a power-law spectrum with intrinsic absorption of $3 - 85 \times 10^{22}$ H-atom cm^{-2} at the source redshift when the power law index was fixed at Γ=2.0 for the combined spectrum of the A + B (source 2) images (G. Chartas et al. 2001). The spectral re-analysis of D. Schwartz et al. (2021) used 24 X-ray photons adding the three images and, assuming a power law photon index of 1.7, confirmed intrinsic absorption of ∼10^{23} H-atom cm^{-2} for the lumped spectrum.

3. *Chandra* SPECTRA

We used `ds9` (W. A. Joye & E. Mandel 2003) to display each of the ten new observations and placed an 0.″90 radius circle about each of the distinct lensed images A, B, and C, where the blended X-ray image C corresponds to two radio images identified by A. More et al. (2009). These circles have about an 80% encircled-count-fraction radius. We used the `ciao 4.17` (A. Fruscione et al. 2006) tool `dmhedit` to correct the RA_NOM and DEC_NOM values of each observation by the difference between the VLBI coordinates of the images and the celestial coordinate that the *Chandra* aspect solution reported for the centroid[4] of each circle. More precisely, the average difference for the three images was used. We used the script `reproject_events` to correct the tangent plane of each obsid to that of Obsid 28556, and then `dmmerge` to merge all 10 observations. ObsID 28556 was chosen as the reference based on having the longest exposure time. Figure 1 shows the merged image with the regions selected for spectral analysis.

Only *Chandra* has sufficient angular resolution to spatially resolve different lensed images of gravitationally lensed AGN systems (with image separations $\lesssim 1.''0$). For MG B2016+112 we carry out separate spectral analyses for the spectra of source 1 and of source 2.

Figure 2 shows the light curve of the measured (magnified) 0.5 – 7 keV flux of the two sources, grouped as identified in Table 1. The flux is derived by fitting each observation to a power-law plus absorption by our galaxy, plus intrinsic absorption at the source redshift. As described below, this is the best fit for each source, although the data does not rule out that source 2 has no intrinsic absorption. To convert to intrinsic luminosity, source 1 (2) – blue (red) in Fig 2 – should be divided by ∼350 (∼2) to correct for the lensing

[4] We determine the centroid using the center of mass algorithm in ds9 after drawing a 0.″9 radius circle by eye around each image. We set 50 iterations, and tolerance of 0.1 pixel per iteration.

Table 1. *Chandra* X-ray observations of MG B2016+112.

Obs ID	Live time (ks)	Counts[a]	Start Date	Group[b]
28554	9.54	17	2023-12-22	1
29135	9.95	14	2023-12-23	1
29136	9.95	16	2023-12-23	1
28556	29.68	49	2024-10-06	2
28141	25.73	46	2024-10-15	2
30569	25.73	45	2024-10-16	2
28555	14.40	36	2024-12-04	3
30645	14.88	34	2024-12-04	3
28557	10.93	18	2025-03-10	4
30844	13.89	31	2025-03-11	4
Sum	164.68	306		

[a] Number of X-ray counts (0.5 - 7 keV observed band) summed in circles of radii 0.″90 about all three images in each ObsID.

[b] The observations within one month are grouped for the light curve displayed in Figure 2.

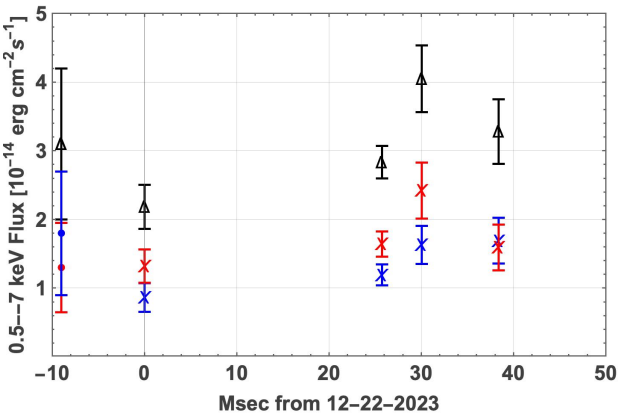


Figure 2. Light curve of all *Chandra* observations of each of the two X-ray sources of MG B2016+112. Observations are grouped as indicated in column 5 of Table 1. Blue "X" points are source 1, image C. Red "X" points are source 2, the sum of images A and B. Error bars are 1σ derived from the square root of the number of counts. We plot the measured 0.5 – 7 keV flux, i.e., the magnified flux from 2.1 – 30 keV in the quasar rest frame, in units of 10^{-14} erg cm^{-2} s^{-1}. Time is measured positively from 23 December 2023. The points plotted at -9 Ms were measured in the archival 7.8 ks observation on 12 April 2000. The black triangles sum the measured counts from all images, as is necessary to compare to observations by any other X-ray telescope.

magnification (C. Spingola et al. 2019), giving intrinsic rest frame 2 – 30 keV luminosities of 3.6×10^{42} and 8.3×10^{44} erg s^{-1} for source 1 and 2, respectively. Neither source is significantly variable, and the two source fluxes are consistent with being the same in each observation. The near equality of the two measured fluxes must be a coincidence, since their magnification factors are so different. *XMM-Newton* observed this source three times in October 2002. Converting the 0.2-12 keV absorbed fluxes listed on the ESA/XMM archive to the 0.5 – 7 keV band using a fixed $\Gamma = 1.7$ and intrisic absorption n_H=3.4×10^{23}cm^{-2} gives an average flux $(3.3 \pm 0.3) \times 10^{-14}$ erg cm $^{-2}$ s^{-1}, consistent with the flux measured by *Chandra* being constant over the entire $\sim$ 25-year observation interval (5.7 years in the source frame; Figure 2).

We used the `ciao 4.18` tool `specextract` to recover photons in regions of 0.″9 radius about each of the three images, for each observation interval (Table 1). The tool formulates the correct absolute response function (the area response file or ARF) and redistribution matrix (RMF) for the appropriate observation date and the actual location on the ACIS-S CCD. We used `combine_spectra` to create a single spectral file for each source. This yielded 139 and 167 total counts for source 1 and source 2, respectively. The background is 0.16 count arcsec^{-2}, so only 1 count out of the 306 used for spectral analysis. Each source has its corresponding files extracted from each ObsID, and each spectrum is analyzed jointly for the 10 observation intervals.

We used `sherpa 4.18.0` (A. Siemiginowska et al. 2024) and `CALDB 4.12.3` to do the spectral fitting, and report the one sigma error on parameters unless otherwise noted. We use the "Cash" statistic on unbinned data (W. Cash 1979). All fits used a Galactic absorption frozen at $n_H = 1.3\times10^{21}$ H-atom cm^{-2} (HI4PI Collaboration et al. 2016). Table 2 shows all of our spectral fitting results.

We first fit a simple power law using the photon spectrum $dN/dE = Ae^{-\sigma(E)*n_H}E^{-\Gamma}$; i.e., the model `xsphabs*powlaw1d` in `sherpa`. The spectral indices for each observation or grouped observation of each source are consistent with the joint fit to all observations. Those photon indices for the joint fits to the ten observations are exceptionally flat: $\Gamma = 1.12 \pm 0.20$ for source 1 and $\Gamma = 1.07 \pm 0.18$ for source 2.

The extremely flat spectrum is more likely due to intrinsic absorption associated with the source. We use the model `xsphabs*xszphabs*powlaw1d` fixing the redshift at z=3.273 and fitting each source separately for the intrinsic column density, photon index, and power law normalization. For source 1 the photon index is $\Gamma = 2.54 \pm 0.21$ with n_H=72 $\times10^{22}$H-atom cm^{-2}. The likelihood value relative to the fit with no intrinic absorption decreases by 10.5, so for the one degree of freedom added this fit is significantly preferred over a power-law with no intrinsic absorption to a confidence of 99.9%, slightly higher than 3σ probability. Source 2 is best fit with a photon index of $\Gamma = 1.46 \pm 0.18$ and intrinsic absorption at the redshift of the source of n_H=22 $\times10^{22}$H-atom cm^{-2}. In this case the one additional parameter of intrinsic absorption only decreases the likelihood function by 1.3, which has a 25% probability of happening by chance, so this fit is not a significant improvement over a simple power law. Figure 3 shows the spectra of the two sources fit with intrinsic absorption.

We consider a maximum likelihood ratio test for the allowed values of the n_H parameter of interest. The ΔLikelihood is distributed as χ^2 with one degree of freedom (S. S. Wilks 1938). The contours in Figure 4 delineate the regions that correspond to 1, 2, and 3 σ probability of enclosing the true parameter region. Source 1 formally excludes n_H=0 to 3.2σ equivalent probability, with a 3σ lower limit $n_H > 4 \times 10^{22}$ H-atoms cm^{-2}. Source 2 is allowed to have zero absorption local to the source for a sufficiently flat photon index, $\Gamma < 1.7$, although within statistics its spectrum also could be the same as source 1.

Quasars will generally be found in the shaded region, with indices between 1 and 3 (D. W. Just et al. 2007; M. Young et al. 2009) and any amount of intrinsic absorption (G. Risaliti et al. 2002, 2009; C. Ramos Almeida & C. Ricci 2017). Jet knots outside of the dusty torus should not show absorption substantially more than that in the line of sight through our galaxy (D. M. Worrall 2009).

4. DISCUSSION AND CONCLUSIONS

The goal of this observation was to determine whether source 1 is an AGN. Source 2 was known to be an AGN due to the observation of broadened emission lines (T. Yamada et al. 2001) and known to host a jet (C. Spingola et al. 2019). Multi-epoch VLBI lens modeling by C. Spingola et al. (2019) had preferred a dual AGN interpretation for sources 1 & 2, but could not rule out that source 1 was a jet (emitted from source 2), being highly magnified ($\mu \sim 350$) when crossing the inner caustic. The work of D. Schwartz et al. (2021) confirmed the existence of two distinct X-ray sources, but the archival *Chandra* observations did not have sufficient counts to measure the individual X-ray spectra of each source. These results motivated the new *Chandra* observations we have presented, specifically to measure intrinsic X-ray absorption in source 1.

Table 2. Fits to spectral models of the two MG B2016+112 sources.

	Source 1 (C)		Source 2 (A+B)	
model	photon index Γ	n_H [a]	photon index Γ	n_H [a]
Power Law (PL)	1.12±0.20	-	1.07±0.18	-
PL + Abs[b]	2.54±0.21	72±20[d]	1.46±0.18	19^{+15}_{-12} [d]
PL + Abs[b]	1.7[c]	34±10	1.7[c]	30^{+18}_{-10} [d]

[a] Intrinsic absorption at the source redshift, in 10^{22} H-atom cm^{-2}

[b] Power law plus intrinsic absorption. See Figure 4 to best assess the errors on the correlated slope and absorption parameters.

[c] Photon index fixed at 1.7

[d] 1σ error assuming the photon index is fixed.

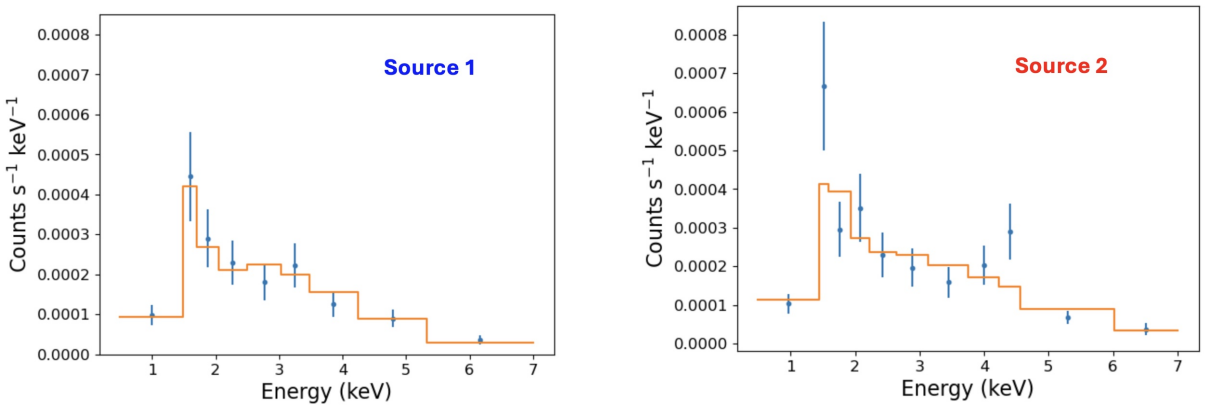


Figure 3. The orange histograms show the models of a power-law with absorption in our galaxy, modified by intrinsic absorption local to the source at the redshift 3.273, folded through the expected mirror and detector response. The x-axis shows the observed energy. For the purpose of display only, the data have been binned into groups of 16 counts per energy channel. The error bars are 1σ derived from the square root of the number of counts. The orange histogram shows the predicted counts per keV in each bin for the best fit photon power law index Γ and intrinsic absorption n_H, and gives the width in energy for each point. Left panel: source 1 with $\Gamma = 2.54 \pm 0.21$ and n_H=72 $\times 10^{22}$H-atom cm^{-2}. Right panel: source 2 with $\Gamma = 1.46 \pm 0.18$ and n_H=19 $\times 10^{22}$H-atom cm^{-2}.

We measure a large intrinsic X-ray absorption of source 1, with a 3σ lower limit $N_H > 4 \times 10^{22}$ H-atoms cm^{-2}, which unambiguously identifies source 1 as an obscured AGN. Absorption in AGN is generally attributed to a dusty torus, at distances less than 10 pc from the SMBH (e.g. Y.-J. Chen et al. 2023; A. K. Mandal et al. 2024). The measured absorption cannot arise from reprocessing in the torus of source 2 (that is, at a distance of at least 175 pc in projection). Therefore, both X-ray emission regions identified by D. Schwartz et al. (2021) originate from two separate AGN.

The ACIS-S response below 2 keV can be precluded as a source of potential bias in measuring the absorption. The ACIS-S response is increasingly reduced at energies below 2 keV, where intrinsic absorption effects are most pronounced. However, this is accounted for in the time-dependent calibration data base maintained by the *Chandra* X-ray Center (D. E. Graessle et al. 2006), and evident in the orange histograms of Figure 3 which show the predicted response to the given source models. Figures 6.4 and 6.8 of the relevant *Chandra* Proposer's Guide[5] show the ACIS-S3 response extending below 1 keV, and the good statistics from observation of the galaxy cluster Abell 1795 that are used to calibrate the response. We note that for recent ACIS ob-

[5] https://cxc.harvard.edu/proposer/POG/arch_pdfs/POG_cyc27.pdf

servations of high redshift quasars both large intrinsic absorptions $> 10^{22}$ cm^{-2} are measured (e.g. P. Breiding et al. 2026) as well as measured limits less than 10^{22} cm^{-2} (e.g. A. Marlar et al. 2025) to column densities. Finally, we note that the present measurement of absorption is consistent with the one on 12 April, 2000 (G. Chartas et al. 2001; D. Schwartz et al. 2021) when the ACIS filter was essentially uncontaminated.

With the confirmation of source 1 as an AGN, we have confirmed the dual AGN nature of MG B2016+112, making this the closest separation AGN pair known at high redshift. All massive galaxies are expected to harbor a central SMBH. When these galaxies merge, their SMBHs may experience a dual AGN phase. Dynamical friction may reduce the distance between the two SMBHs, to the extent that the two systems may eventually form a gravitationally bound pair and merge (K. Li et al. 2020a,b). The galaxy merging process is expected to provide gas supply, possibly triggering AGN activity in both SMBH (S. Burke-Spolaor et al. 2018; L. Mayer et al. 2007).

Although cosmological simulations predict such systems (M. Tremmel et al. 2018; Y. M. Rosas-Guevara et al. 2019; M. Volonteri et al. 2022; N. Chen et al. 2023), direct observational evidence has remained elusive. Until now, dual AGNs with sub-kiloparsec separations had been observed only at low redshift, leaving scarce direct evidence for such systems at or beyond the peak of galaxy evolution (J. M. Comerford et al. 2012; A. De Rosa et al. 2018; Y.-C. Chen et al. 2022, 2025; H. Suh et al. 2026). The system MG B2016+112 presented here, with a projected separation of only 175 pc, is the first of its kind and provides a unique probe of hierarchical galaxy evolution. Its detection was enabled by strong gravitational lensing, which both magnified the source flux and spatially magnified the system. Without this combined flux and spatial magnification, the source would have been too faint and its two components too compact to resolve. Lensing therefore provided the sensitivity and effective source-plane resolution required to identify the two AGNs and measure their 175 pc projected separation at $z = 3.237$.

Determining the fraction of dual AGN and their circumnuclear environments is critical for estimating galaxy merger rates in the early universe, and also for assessing the time scales for SMBH pairs to coalesce and emit gravitational waves. A. De Rosa et al. (2019) and T. Bogdanović et al. (2022) review techniques for identifying dual and binary SMBH. Estimates of dual AGN found in a single galaxy subsequent to a merger are uncertain, with a range of at least 1% (M. Volonteri et al. 2022) to 20 – 30% (M. Perna et al. 2025).

Searches for dual AGN are currently of great interest, enhanced by the intial data releases from *Euclid* and *SKA*, and the commissioning of the *Rubin* and *Roman* observatories. These facilities allow detections of pairs of radio and optical sources at separations below a kpc. L. Ulivi et al. (2025) applied machine learning methods to Euclid data to reveal quasar candidates that could be either dual AGN or lensed AGN. Q. D'Amato et al. (2026) make the case for the SKAO identifying pairs with projected separations of only several hundred pc at large redshift. One can then use high resolution X-ray imaging and spectroscopy to provide critical diagnostics for confirming AGN pair candidates as either dual or lensed systems. In parallel, gravitationally lensed AGN pairs at high redshift may be directly revealed via X-ray astrometry.

This work has been supported by NASA contract NAS8-03060 to SAO, NASA/ADAP grant 80NSSC24K0617, and grant GO4-25053X from the CXC. This research made use of the NASA Astrophysics Data System, now the SciX Digital Library, funded by NASA under Cooperative Agreement 80NSSC21M00561. We thank D. Burke for assistance with `sherpa`. We thank Giulia Migliori, Cristiana Spingola, and Mauro Dadina for calling our attention to the XMM observation.

Facilities: Chandra (ACIS)

Software: ciao-4.17, ciao-4.18 (A. Fruscione et al. 2006), sherpa-4.18 (A. Siemiginowska et al. 2024; D. Burke et al. 2025), SAOImageDS9 Version 8.4.1 (W. A. Joye & E. Mandel 2003), APLpy (T. Robitaille & E. Bressert 2012), SAOTrace - 2.0.6.1 (D. H. Jerius et al. 2004), Marx - 6.0.1 (J. E. Davis et al. 2012).

REFERENCES

Barnacka, A. 2017, ApJ, 846, 157, doi: 10.3847/1538-4357/aa86ec

Barnacka, A. 2018, Phys. Rep., 778, 1, doi: 10.1016/j.physrep.2018.10.001

Bogdanović, T., Miller, M. C., & Blecha, L. 2022, Living Reviews in Relativity, 25, 3, doi: 10.1007/s41114-022-00037-8

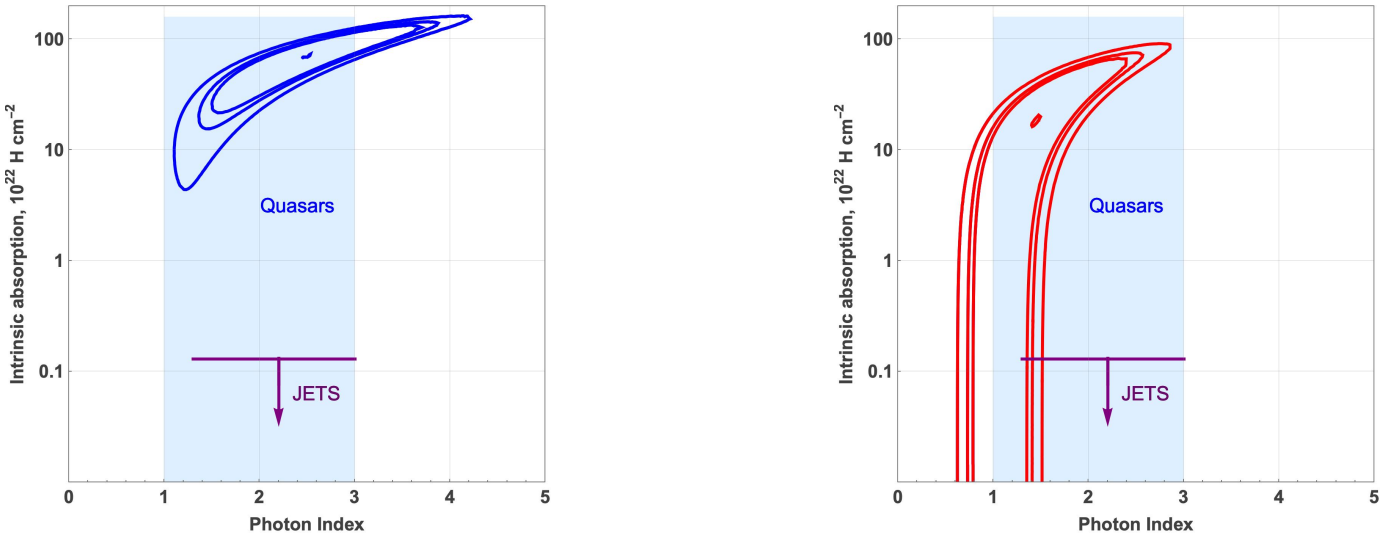


Figure 4. The left panel shows source 1 and the right panel source 2. The contour plots show allowed combinations of the correlated parameters of intrinsic absorption and photon power law index. The contours from innermost to outermost delineate regions of 1, 2, and 3 σ probability that the data could arise from such a pair of parameters, when marginalized over the uninteresting parameters of photon index and the normalization. The central dots show the best parameters from the spectra in figure 3. The shaded blue region is indicative of the location of most quasars. The purple down-arrow indicates the allowed region for jets, with the bar at the n_H=1.3×10^{21} galactic column density that would allow no excess over the galactic column in this direction.

Breiding, P., Eracleous, M., Bogdanović, T., Burke-Spolaor, S., & Lazio, T. J. W. 2026, arXiv e-prints, arXiv:2602.20438, doi: 10.48550/arXiv.2602.20438

Burke, D., Laurino, O., McLaughlin, W., et al. 2025, Zenodo, doi: 10.5281/zenodo.17288983

Burke-Spolaor, S., Blecha, L., Bogdanović, T., et al. 2018, in Astronomical Society of the Pacific Conference Series, Vol. 517, Science with a Next Generation Very Large Array, ed. E. Murphy, 677

Cash, W. 1979, ApJ, 228, 939, doi: 10.1086/156922

Chartas, G., Bautz, M., Garmire, G., Jones, C., & Schneider, D. P. 2001, ApJL, 550, L163, doi: 10.1086/319632

Chen, N., Di Matteo, T., Ni, Y., et al. 2023, MNRAS, 522, 1895, doi: 10.1093/mnras/stad834

Chen, Y.-C., Gross, A. C., Liu, X., et al. 2025, ApJ, 988, 126, doi: 10.3847/1538-4357/ade23b

Chen, Y.-C., Hwang, H.-C., Shen, Y., et al. 2022, ApJ, 925, 162, doi: 10.3847/1538-4357/ac401b

Chen, Y.-J., Liu, J.-R., Zhai, S., et al. 2023, MNRAS, 522, 3439, doi: 10.1093/mnras/stad1136

Comerford, J. M., Gerke, B. F., Stern, D., et al. 2012, ApJ, 753, 42, doi: 10.1088/0004-637X/753/1/42

D'Amato, Q., Cui, L., Deane, R., et al. 2026, arXiv e-prints, arXiv:2606.28512, doi: 10.48550/arXiv.2606.28512

Davis, J. E., Bautz, M. W., Dewey, D., et al. 2012, in Society of Photo-Optical Instrumentation Engineers (SPIE) Conference Series, Vol. 8443, Space Telescopes and Instrumentation 2012: Ultraviolet to Gamma Ray, ed. T. Takahashi, S. S. Murray, & J.-W. A. den Herder, 84431A, doi: 10.1117/12.926937

De Rosa, A., Vignali, C., Husemann, B., et al. 2018, MNRAS, 480, 1639, doi: 10.1093/mnras/sty1867

De Rosa, A., Vignali, C., Bogdanović, T., et al. 2019, New Astronomy Reviews, 86, 101525, doi: 10.1016/j.newar.2020.101525

Di Matteo, T., Colberg, J., Springel, V., Hernquist, L., & Sijacki, D. 2008, ApJ, 676, 33, doi: 10.1086/524921

Fruscione, A., McDowell, J. C., Allen, G. E., et al. 2006, in Society of Photo-Optical Instrumentation Engineers (SPIE) Conference Series, Vol. 6270, Society of Photo-Optical Instrumentation Engineers (SPIE) Conference Series, ed. D. R. Silva & R. E. Doxsey, 62701V, doi: 10.1117/12.671760

Graessle, D. E., Evans, I. N., Glotfelty, K., et al. 2006, in Society of Photo-Optical Instrumentation Engineers (SPIE) Conference Series, Vol. 6270, Observatory Operations: Strategies, Processes, and Systems, ed. D. R. Silva & R. E. Doxsey, 62701X, doi: 10.1117/12.672876

HI4PI Collaboration, Ben Bekhti, N., Flöer, L., et al. 2016, A&A, 594, A116, doi: 10.1051/0004-6361/201629178

Hopkins, P. F., Hernquist, L., Cox, T. J., & Kereš, D. 2008, ApJS, 175, 356, doi: 10.1086/524362

Jerius, D. H., Cohen, L., Edgar, R. J., et al. 2004, in Optical Science and Technology, SPIE's 48th Annual Meeting, San Diego, California, USA, 402, doi: 10.1117/12.509378

Joye, W. A., & Mandel, E. 2003, in Astronomical Society of the Pacific Conference Series, Vol. 295, Astronomical Data Analysis Software and Systems XII, ed. H. E. Payne, R. I. Jedrzejewski, & R. N. Hook, 489

Just, D. W., Brandt, W. N., Shemmer, O., et al. 2007, ApJ, 665, 1004, doi: 10.1086/519990

Koopmans, L. V. E., Garrett, M. A., Blandford, R. D., et al. 2002, MNRAS, 334, 39, doi: 10.1046/j.1365-8711.2002.05438.x

Li, K., Bogdanović, T., & Ballantyne, D. R. 2020a, ApJ, 896, 113, doi: 10.3847/1538-4357/ab93c6

Li, K., Bogdanović, T., & Ballantyne, D. R. 2020b, ApJ, 905, 123, doi: 10.3847/1538-4357/abc555

Li, Q., Conselice, C. J., Duan, Q., et al. 2025, MNRAS, 544, 4160, doi: 10.1093/mnras/staf1992

Mandal, A. K., Woo, J.-H., Wang, S., et al. 2024, ApJ, 968, 59, doi: 10.3847/1538-4357/ad414d

Mannucci, F., Pancino, E., Belfiore, F., et al. 2022, Nature Astronomy, 6, 1185, doi: 10.1038/s41550-022-01761-5

Mannucci, F., Scialpi, M., Ciurlo, A., et al. 2023, A&A, 680, A53, doi: 10.1051/0004-6361/202346894

Marlar, A., Shemmer, O., Brotherton, M. S., et al. 2025, ApJ, 991, 91, doi: 10.3847/1538-4357/adf4dd

Massaro, F., Harris, D. E., & Cheung, C. C. 2011, ApJS, 197, 24, doi: 10.1088/0067-0049/197/2/24

Mayer, L., Kazantzidis, S., Madau, P., et al. 2007, Science, 316, 1874, doi: 10.1126/science.1141858

More, A., McKean, J. P., More, S., et al. 2009, MNRAS, 394, 174, doi: 10.1111/j.1365-2966.2008.14342.x

Perna, M., Arribas, S., Lamperti, I., et al. 2025, A&A, 696, A59, doi: 10.1051/0004-6361/202453430

Planck Collaboration, Aghanim, N., Akrami, Y., et al. 2020, A&A, 641, A6, doi: 10.1051/0004-6361/201833910

Ramos Almeida, C., & Ricci, C. 2017, Nature Astronomy, 1, 679, doi: 10.1038/s41550-017-0232-z

Risaliti, G., Elvis, M., & Nicastro, F. 2002, ApJ, 571, 234, doi: 10.1086/324146

Risaliti, G., Young, M., & Elvis, M. 2009, ApJL, 700, L6, doi: 10.1088/0004-637X/700/1/L6

Robitaille, T., & Bressert, E. 2012, http://ascl.net/1208.017

Rosas-Guevara, Y. M., Bower, R. G., McAlpine, S., Bonoli, S., & Tissera, P. B. 2019, MNRAS, 483, 2712, doi: 10.1093/mnras/sty3251

Schneider, D. P., Gunn, J. E., Turner, E. L., et al. 1986, AJ, 91, 991, doi: 10.1086/114075

Schwartz, D., Spingola, C., & Barnacka, A. 2021, ApJ, 917, 26, doi: 10.3847/1538-4357/ac0909

Siemiginowska, A., Burke, D., Günther, H. M., et al. 2024, ApJS, 274, 43, doi: 10.3847/1538-4365/ad7bab

Space Telescope Science Institute. 2023, Hubble Space Telescope Instrument Handbook, Space Telescope Science Institute, Baltimore, MD. https://hst-docs.stsci.edu/

Spingola, C., McKean, J. P., Massari, D., & Koopmans, L. V. E. 2019, A&A, 630, A108, doi: 10.1051/0004-6361/201935427

Suh, H., Decarli, R., Farina, E. P., et al. 2026, arXiv e-prints, arXiv:2607.19491, doi: 10.48550/arXiv.2607.19491

Tremmel, M., Governato, F., Volonteri, M., Quinn, T. R., & Pontzen, A. 2018, MNRAS, 475, 4967, doi: 10.1093/mnras/sty139

Ulivi, L., Mannucci, F., Scialpi, M., et al. 2025, arXiv e-prints, arXiv:2508.19494, doi: 10.48550/arXiv.2508.19494

Volonteri, M., Pfister, H., Beckmann, R., et al. 2022, MNRAS, 514, 640, doi: 10.1093/mnras/stac1217

Wilks, S. S. 1938, Ann. Math Stat., 9, 60

Worrall, D. M. 2009, A&A Rv, 17, 1, doi: 10.1007/s00159-008-0016-7

Yamada, T., Yamazaki, S., Hattori, M., Soucail, G., & Kneib, J. P. 2001, A&A, 367, 51, doi: 10.1051/0004-6361:20000418

Young, M., Elvis, M., & Risaliti, G. 2009, ApJS, 183, 17, doi: 10.1088/0067-0049/183/1/17